Cilia-driven fluid flow in the zebrafish pronephros, brain and Kupffer's vesicle is required for normal organogenesis

Albrecht G. Kramer-Zucker[1], Felix Olale[2], Courtney J. Haycraft[3], Bradley K. Yoder[3], Alexander F. Schier[2] and Iain A. Drummond[1,*]

[1]Renal Unit, Massachusetts General Hospital, 149 13th Street, Charlestown, MA 02129, USA
[2]Developmental Genetics Program, Skirball Institute of Biomolecular Medicine, New York University School of Medicine, New York, NY 10016, USA
[3]Department of Cell Biology, University of Alabama at Birmingham Medical Center, Birmingham, AL 35294, USA
*Author for correspondence (e-mail: idrummon@receptor.mgh.harvard.edu)

Accepted 4 February 2005

Development 132, 1907-1921
Published by The Company of Biologists 2005
doi:10.1242/dev.01772

Summary

Cilia, as motile and sensory organelles, have been implicated in normal development, as well as diseases including cystic kidney disease, hydrocephalus and situs inversus. In kidney epithelia, cilia are proposed to be non-motile sensory organelles, while in the mouse node, two cilia populations, motile and non-motile have been proposed to regulate situs. We show that cilia in the zebrafish larval kidney, the spinal cord and Kupffer's vesicle are motile, suggesting that fluid flow is a common feature of each of these organs. Disruption of cilia structure or motility resulted in pronephric cyst formation, hydrocephalus and left-right asymmetry defects. The data show that loss of fluid flow leads to fluid accumulation, which can account for organ distension pathologies in the kidney and brain. In Kupffer's vesicle, loss of flow is associated with loss of left-right patterning, indicating that the 'nodal flow' mechanism of generating situs is conserved in non-mammalian vertebrates.

Key words: Cilia, Pronephros, Kupffer's vesicle, Ependymal cell, Spinal canal, Kidney cyst, Hydrocephalus, Left-right asymmetry

Introduction

Cilia and flagella have well-established roles as motile and sensory organelles in various species; however, their function in vertebrate organogenesis is only now coming to light. The identification of mutations in ciliogenic genes as the underlying cause of several mutant phenotypes and human pathologies, including polycystic kidney disease, left-right asymmetry defects and retinal degeneration, has implicated cilia function in the normal development of several organs (Ibanez-Tallon et al., 2003).

The establishment of left-right asymmetry is the earliest embryonic process associated with cilia function. To generate proper organ laterality, mechanisms must exist that translate existing anterior-posterior polarity into signals that break the bilateral symmetry of the gastrulating embryo. The asymmetric expression of genes such as *nodal* and *southpaw* (Bisgrove et al., 2003; Hamada et al., 2002) and the position of organs such as the heart on the left side of the trunk reflect the outcome of early left-right signaling. In humans, abnormalities in organ situs in the primary ciliary dyskinesia (PCD) syndrome (Afzelius, 1985) are due to mutations in several different axonemal dyneins affecting ciliary motility (Ibanez-Tallon et al., 2003). The *inversus viscerum* (*iv*) mouse, which is mutant in the left-right dynein gene (*lrd*; *Dnahc11* – Mouse Genome Informatics) encoding an axonemal dynein heavy chain present in node cilia (Supp et al., 1997), displays randomization of early gene expression and later organ laterality (Layton, 1976; Lowe et al., 1996). Cilia paralysis and loss of fluid flow in this and other mutants (Brody et al., 2000; Chen et al., 1998; Marszalek et al., 1999; Nonaka et al., 1998) suggested that nodal fluid flow was the key factor in establishing organ situs. Artificial reversal of nodal flow has been shown to randomize the left-right axis, providing further support for the 'nodal flow' hypothesis (Nonaka et al., 2002). McGrath and co-workers have proposed that two types of cilia exist in the node: motile *lrd*-expressing cilia and non-motile *polycystin2*-expressing sensory cilia (McGrath et al., 2003). Nodal flow could generate a morphogen gradient regulating situs, or, alternatively, mechanosensory ion fluxes mediated by *polycystin2* may be the signal that initiates left-sided gene expression. Whatever the final signal may be, the demonstration that dynein-expressing node monocilia exist in a range of vertebrate embryos (Brummett and Dumont, 1978; Essner et al., 2002) indicates that cilia-driven fluid flow may be part of a general mechanism for establishing left-right asymmetry. Currently, however, 'nodal flow' has been directly demonstrated only in mouse embryos, and it is unclear whether or not ciliary motion and fluid flow is relevant to other vertebrates.

Cilia dysfunction has been implicated in polycystic kidney disease, based on the findings that disruption of ciliogenic and cilia-associated genes leads to cyst formation in the kidney (Igarashi and Somlo, 2002; Nauli and Zhou, 2004). The two proteins associated with human autosomal dominant PKD, Polycystin-1 and Polycystin-2, have been detected in the renal

cilium (Pazour et al., 2002; Yoder et al., 2002) as has the product of the *inversin* gene, which is mutant in the human kidney cystic condition nephronophthisis type 2 (Otto et al., 2003). Cystin, the protein encoded by the mutant gene in the cpk cystic mouse, is also localized to apical cilia (Hou et al., 2002; Yoder et al., 2002). In zebrafish, the results of a large-scale retroviral insertional mutagenesis screen revealed that several genes associated with cilia assembly were mutated in fish that developed pronephric cysts (Sun et al., 2004). In mammalian epithelial cultured cells, cilia are proposed to be non-motile mechanosensors that initiate signals controlling tubular epithelial cell proliferation or homeostasis (Nauli et al., 2003; Pazour and Witman, 2003). Non-motile cilia with sensory functions have been described in *Caenorhabditis elegans* neurons and several mutant strains with altered sensory behavior have been identified (Perkins et al., 1986). However, whether kidney cilia are always immotile, or whether they might play an additional role in kidney tubule fluid movement, remains an unresolved question.

Our insight into cilia assembly has been significantly advanced by the discovery of the cellular machinery responsible for moving particles along the microtubule scaffold of cilia or flagella, called intraflagellar transport (IFT) (Rosenbaum and Witman, 2002). The pleiotropic phenotype observed in animals carrying mutations in IFT genes has confirmed the importance of cilia in organogenesis and tissue physiology. A hypomorphic mutation in the mouse *polaris* gene (*Tg737/IFT88*) results in cystic kidney disease, pancreatic and bile duct hyperplasia, hydrocephalus, and skeletal patterning defects (Cano et al., 2004; Moyer et al., 1994; Richards et al., 1996; Yoder et al., 1995). In zebrafish, the *oval* mutant is a stop codon in the *polaris/IFT88* homolog; these fish show widespread neurosensory cell death (Tsujikawa and Malicki, 2004). Three different zebrafish IFT proteins associated with cystic kidneys were also identified in a large-scale insertional mutagenesis screen (Sun et al., 2004). Despite the implication that cilia defects are associated with mutant phenotypes, the mechanism by which ciliary malfunction may lead to the various organ pathologies remains unclear.

To better understand the developmental roles of cilia in organogenesis, we examined cilia in the pronephric kidney, the spinal cord and Kupffer's vesicle (KV, the equivalent of the mouse embryonic node) of zebrafish larvae and assessed the consequence that loss of cilia has on the formation and function of these organs. We found that cilia in all three of these structures are motile, suggesting that cilia function to drive fluid flow. Indeed, we show by using injected fluorescent tracers that this is the case. Disruption of cilia function in IFT morphant embryos resulted in loss of fluid flow and subsequent development of kidney cysts, hydrocephalus and laterality defects. The association between defects in fluid flow and organ pathology when cilia biogenesis was perturbed suggests that a common mechanism, namely loss of fluid flow, leads to fluid backup and subsequent organ distension, with formation of cysts in the kidney and hydrocephalus in the brain. Our data also demonstrate that fluid flow is a conserved feature of gastrulation-stage midline structures that regulate left-right asymmetry and, further, that disruption of this flow in zebrafish also causes abnormalities in situs.

Materials and methods

Zebrafish lines

Wild-type TL or TÜAB zebrafish were maintained and raised as described (Westerfield, 1995). Dechorionated embryos were kept at 28.5°C in E3 solution with or without 0.003% 1-Phenyl-2-thiourea (PTU, Sigma) to suppress pigmentation and staged according to somite number (som) or hours post-fertilization (hpf) (Westerfield, 1995).

Cloning of *polaris*, *hippi* and a fragment of pronephric axonemal *dynein heavy chain 9*

Zebrafish *polaris* was cloned by RT-PCR based on sequence predicted from Sanger Center zebrafish genomic DNA sequence (Sanger Institute). RT-PCR products were subcloned in pCRII TOPO (Invitrogen) and sequenced. Zebrafish *hippi* sequence was derived partially by tblastn searches (Sanger Institute) and used for 5′ and 3′ RACE reactions (Invitrogen). Finally, the coding sequence was obtained by reverse transcription and nested PCR of wild-type total RNA (outer primer-set: forward CCCTTTGCGAGTAAAGAGTGTTAAATGTGA, reverse CATCATCTGCTGCAAACTAGCCCTCT, nested primer-set forward CGGGATCC*GCCACC*ATGGCGGAGGAGGAAGAG reverse CGGAATTCCGGCGGTGAGTGTGTGTTTCAATA) and subcloned into the expression vector pCS2+. The *hippi* gene maps to linkage group 2. The nested PCR for murine *hippi* was performed based on known sequence in GenBank (NM_028680) using total RNA from mouse brain (kind gift from Dr Ruth Luthi-Carter, Neurology, MGH) and the following primer (outer primer-set: forward GGCGCTGGGGGTCTGAGCA, reverse AAATTGTGTTTGGAAATCAATGCAACA, nested primer-set forward CGGAATTCGCCACCATGGCCGCCGCGGCCGCG, reverse GCTCTAGAGAAGCATGGAAGCCCACGTGTTTA). The amplicon was subcloned into the expression vector pCS2+.

For isolation of pronephros specific axonemal dynein heavy chains, 72 hpf. zebrafish embryos were incubated in 10 mmol/l DTT in egg water for 1 hour at room temperature and then washed three times with egg water. They were then incubated at 28.5°C in 5 mg/ml collagenase II in Hank's saline with calcium (Worthington) for 4 hours. The larvae were then put in Hank's saline and triturated gently five times with a 1000 μl pipette tip, so that the disintegrated, approximately 20 pronephric duct fragments were collected by visual identification. Total RNA from the collected tissue was used for reverse transcription and nested PCR. The following degenerate primers were used (I=inosine): GTIAT(AC)ACICCICTIACIGA (forward primer), GCIGGIACIGGIAA(AG)ACIGA (nested forward primer), C(GT)ICCIGC(AG)TAICCIGG(AG)TT (reverse primer for reverse transcription and first and second PCR). A 323 bp fragment was subcloned and 15 clones were sequenced.

Accession numbers

ift57/hppi, AY956331; dynein heavy chain 9, AY956332; *ift88/polaris*, AY956333.

In situ hybridization

Whole-mount in situ hybridization was performed as previously described (Thisse and Thisse, 1998) with some minor modifications. For the *polaris* antisense probe the template (pCRII-TOPO-polaris 1200 bp, flanking primers forward AGCAGGCTGTCAGGACAAGTC and reverse GTTTGAAGTCTCTCTGTCTTAGGT was linearized with *Not*1 and the antisense riboprobes were transcribed using SP6 RNA polymerase. The *hippi* antisense riboprobes were generated using a *Bam*HI linearized template and T7 RNA polymerase. In situ hybridization experiments with *southpaw* (*spaw*) (Long et al., 2003) and *pitx2* (Yan et al., 1999) were performed using standard techniques. Embryos were then mounted in Permount (Fisher Scientific) and photographed on a Zeiss Axioplan microscope equipped with a Zeiss AxioCam digital camera.

Morpholino antisense oligonucleotides

Morpholino antisense oligonucleotides were designed either to target the translation of the mRNA (abbreviation AUG) leading to a protein knockdown phenotype or to target an exon splice donor site causing splicing defects of the mRNA (abbreviation SP). For the design of the antisense oligonucleotides the translation start site and the splice donor site of the second coding exon were chosen and the morpholino oligonucleotides obtained from GENE TOOLS, LLC, Philomath, OR. The following morpholinos were used: *polaris*AUG CTGGGACAAGATGCACATTCTCCAT, *polaris*SP AGCAGATG-CAAAATGACTCACTGGG, *hippi*AUG CCTCCGCCATCCCT-CTCTCTTTCT, *hippi*AUGmis CCTgCGgCATCCgTCTCTgTTaCT (5 mismatches in lower case), *hippi*SP AGTGTTATCGCCT-CACCAGGGTTCG, *dhc9*P1SP GATTTACACACCTTGTAGTC-CATTT. The morpholinos were diluted in 100 mmol/l KCl, 10 mmol/l HEPES, 0.1% Phenol Red (Sigma). The injections were done using a microinjector PLI-90 (Harvard Apparatus, Cambridge, MA). The effect of the splice-morpholinos was verified by RT-PCR from single embryo total RNA with nested primers in flanking exons yielding a 300-600 bp amplicon. Rescue experiments were done by co-injection of capped mRNA together with a morpholino. Capped mRNA was made using mMESSAGE mMACHINE (Ambion). For the injection of the capped mRNA or capped mRNA together with morpholino, a microprocessor controlled nanoliter injector Nanoliter 2000 (World Precision Instruments, Inc.) was used.

Histochemistry and immunohistochemistry

Embryos were fixed in 2% glutaraldehyde/1.5% paraformaldehyde/70 mmol/l Na_2HPO_4 pH 7.2/3% sucrose at 4°C overnight. After being washed in PBS and taken through an ethanol dehydration series they were embedded in JB-4 resin (Polysciences Inc.) and sectioned at 3-5 μm. Slides were stained in Methylene Blue/Azure II (Humphrey and Pittman, 1974), mounted and examined using a Nikon immunofluorescence microscope. For acetylated tubulin staining, the embryos were fixed in Dent's Fix (80% methanol/20% DMSO) at 4°C overnight. After gradual rehydration they were washed several times in 1×PBS with 0.5% Tween20 and blocked in 1×PBS-DBT (1% DMSO/1% BSA/0.5% Tween20) with 10% normal goat serum (NGS) (Sigma) at room temperature for 2 hours. Primary antibody incubation in 1×PBS-DBT 10% NGS [1:500 monoclonal anti-acetylated tubulin 6-11B-1 (Piperno and Fuller, 1985) (Sigma)] was at 4°C overnight. The embryos were washed in 1×PBS with 0.5% Tween20 and blocked in 1×PBS-DBT 10% NGS at RT for 1 hour and then incubated in 1:1000 goat anti-mouse Alexa 546 (Molecular Probes) in 1×PBS-DBT 10% NGS at 4°C overnight. After rinsing in 1×PBS, the embryos were washed with methanol and equilibrated in clearing solution (1/3 benzoyl-alcohol and 2/3 benzoyl-benzoate) and examined using a Bio-Rad Radiance 2000 confocal microscope. Z-stacks were acquired and used for creation of projections with extended focus.

Cilia length measurements were performed using Image J 1.32j (National Institute of Health) in two to four different embryos per group. Confocal images where individual cilia base and ends could be discerned (>60 individual measurements) were outlined and the calculated length recorded. Our measurements may underestimate cilia length owing to a foreshortening effect caused by viewing some cilia at an angle.

For double labeling with two monoclonal antibodies, the embryos were stained as above and the procedure was repeated with 1:20 monoclonal antibody alpha 6F, raised against the chicken alpha1 subunit of the Na+/K+ ATPase (Takeyasu et al., 1988), obtained from the Developmental Studies Hybridoma Bank, as primary and 1:1000 goat anti-mouse Alexa 633 (Molecular Probes) as secondary antibody after incubation with goat anti-mouse Fab fragments 1:20 in 1×PBS-DBT at 4°C overnight.

Electron microscopy

Embryos were prepared for electron microscopy by previously published protocols (Drummond et al., 1998).

High speed videomicroscopy

PTU-treated embryos were put in E3 egg water containing 40 mmol/l BDM (2,3-butanedione monoxime, Sigma), for 5 minutes to stop the heartbeat and then changed to 20 mmol/l BDM containing egg water for observation. The embryos were then analyzed using a 40×/0.55 water immersion lens on a Zeiss Axioplan microscope (Zeiss, Germany) equipped with a high-speed Photron FastCAM-PCI 500 videocamera (Photron LTD). Image acquisition of beating cilia was 250 frames per second and 1088 frames total per take by Photron FastCAM version 1.2.0.7 (Photron LTD). Image processing was done using Photoshop 7.0 (Adobe) and movies compiled in Graphic Converter v.4.5.2 (Lemke Software, Germany). Three-dimensional illustrations were drawn using Strata3D Software (Strata).

Fluorescent dye/bead injection and fluorescence videomicroscopy

For urine excretion assays a 5% solution of Tetramethylrhodamin-conjugated 70 k MW dextran (Molecular Probes) was injected into the common cardinal vein (CCV) of 3.0-3.5 dpf. embryos anesthetized with 0.2 mg/ml tricaine (3-aminobenzoic acid ethylester, Sigma) in egg water, these were then examined using a 40×/0.55 water immersion lens on a Zeiss Axioplan microscope equipped with a MTI SIT68 fluorescence camera the video was recorded at real time with a Panasonic PV-8400 tape recorder. Digitalization was done using SonicMyDVD Version 3.5.2 software (Adaptec), still frames were captured using QuickTime v.6.5.1 and movies were recompiled by Graphic Converter (Lemke Software, Germany). For the dye transport in the central canal, the dye was injected into the brain ventricle of 60 hpf. embryos anesthetized with tricaine. Sequential images were taken with a Nikon fluorescence microscope. Fluorescent beads of 0.02 μm diameter (Fluospheres (580/605), Molecular Probes) were dispersed 1:50 in 0.1 mol/l saline with 0.1% Phenol Red (Sigma) and used for injection into KV of embryos at 8-10 somite stage.

Statistics

The two-tailed Student's *t*-test was applied to the quantitative results.

Results

Apical cilia are present in KV, in the central canal of the spinal cord, and in the pronephric ducts

To survey zebrafish larvae for the presence of ciliated cells during organogenesis, we performed immunocytochemistry using an anti-acetylated tubulin antibody. Immunostaining confirmed an earlier report that apical cilia are present in cells lining KV at the 8-somite stage (Fig. 1A,D) (Essner et al., 2002). Also, ependymal cells along the central canal bore apical cilia at 24 hpf (Fig. 1B,E), as did pronephric duct cells at 48 hpf (Fig. 1C,F). KV cilia and pronephric duct cilia showed an ultrastructure consisting of nine peripheral microtubules and a central pair (9+2 pattern; Fig. 1G,I), whereas a 9+0 formation was present in ependymal cell cilia along the central canal of the spinal cord (Fig. 1H). Outer dynein arms were present in cilia of all three organs (arrows). All kidney cilia examined were 9+2; no 9+0 cilia were found in the zebrafish pronephros.

Cilia in pronephros, central canal and KV are motile

The presence of dynein outer arms in the cilia of all three tissues suggested that these cilia are motile (Smith and Yang,

2004). We therefore examined cilia for motility using high-speed videomicroscopy. To examine pronephric cilia, embryos at 2.5 days post-fertilization (dpf) were treated with butanedione monoxime (BDM) to stop the heartbeat and circulation in order to eliminate glomerular filtration pressure. Images were acquired at 250 frames per second and then replayed in slow motion at 15 frames per second to count the beat frequency. Under these conditions, cilia beating at a frequency of 20.0±3.2 Hz (n=34) were observed in all parts of the pronephros, including the tubules and ducts (see Movies 1, 2 in the supplementary material). As a similar cilia beat frequency was observed in embryos not treated with BDM, we conclude that BDM does not influence cilia motility. In BDM-treated embryos there was no luminal fluid flow generated by glomerular filtration, so the observed cilia movements must represent active beating and not passive deflection. Rotational cilia movement generated a corkscrew-like wave pattern in the lumen of the duct directed toward the cloaca (Fig. 1K). While the majority of pronephric epithelial cells displayed a single apical motile cilium, a subset of cells with up to 16 apical cilia could be observed in the midpart of the pronephric duct.

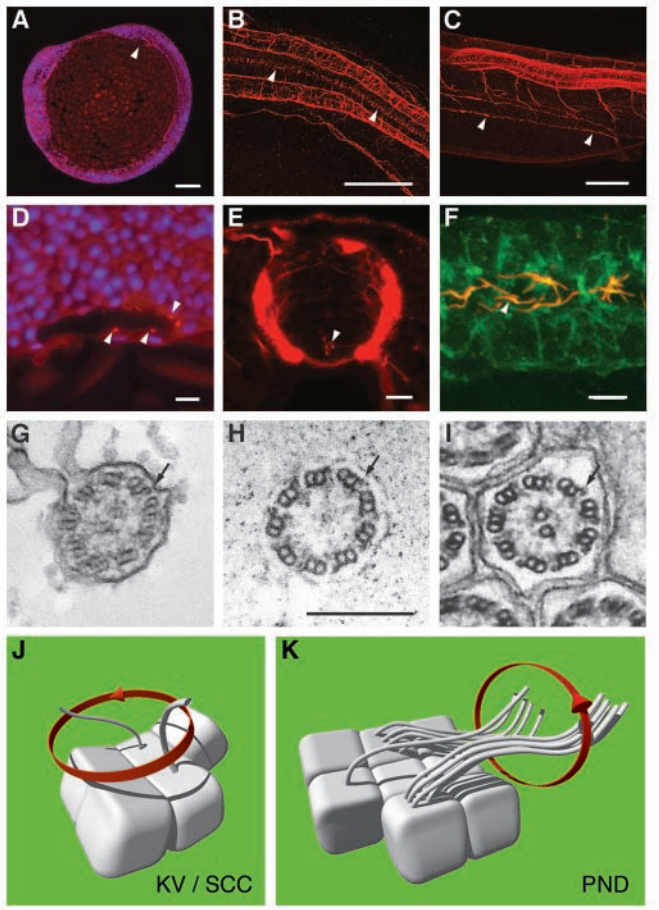

	KV	SCC	PND
length [µm]	3.3 ± 1.1	2.1 ± 0.7	8.8 ± 2.0
frequency [Hz]	26.2 ± 1.6	12.3 ± 3.4	20.0 ± 3.2

Fig. 1. Apical cilia are present in Kupffer's vesicle, the central canal of the spinal cord and pronephric ducts. Immunostaining of acetylated tubulin. (A) Apical cilia are present in cells lining Kupffer's vesicle at the 8-somite stage (arrowhead) in midline longitudinal sections. (D) Kupffer's vesicle; higher magnification (DAPI nuclear staining in blue). (B) Ependymal cells along the central canal bear cilia at 24 hpf (arrowheads). (E) Cross section at 44 hpf; cilia arise from all cells of the spinal central canal. (C) Cilia can also be seen in the pronephric duct at 48 hpf (arrowheads). (F) Cells double stained for acetylated tubulin and the alpha1 subunit of the NaK-ATPase confirmed the apical position of the pronephric cilia. (G-I) EM cross sections of cilia in Kupffer's vesicle (G) show a 9+2 structure; ependymal cell cilia (H) are 9+0 in structure; pronephric cilia (I) are 9+2 with clear dynein outer arms (arrows). Cilia beat pattern: (J) The cilia in the of the spinal central canal and Kupffer's vesicle rotate in an counterclockwise orientation. (K) In the pronephric duct monociliated and multiciliated cells can be observed. Their cilia beat in rotation like a corkscrew with an undulating appearance along their longitudinal axis. Mean values for cilia length and beat frequency are given for comparison. Scale bars: 100 µm in A-C; 10 µm in D-F; 250 nm in G-I. KV, Kupffer's vesicle; PND, pronephric duct; SCC, spinal central canal.

The cilia in the central canal of the spinal cord were filmed under the same BDM conditions as above to avoid disturbances by circulating blood cells. The ependymal cilia were approximately 2 µm in length and also showed a rotary pattern of motility (Fig. 1J). The frequency of rotation was approximately 12 Hz (see Movie 4 in the supplementary material).

The cilia in KV were similar in length (3 µm) to the ependymal cilia and rotated in a counterclockwise orientation (Fig. 1J; see Movie 8 in the supplementary material). In addition to images of moving KV cilia themselves, cilia motility could be detected by the movement of small pieces of debris suspended in the fluid of KV. Debris was observed to travel in a counterclockwise orbit, interrupted by small counterclockwise spins corresponding to the radii of circular cilia beat patterns (see Movie 9 in the supplementary material). This type of particle and fluid movement was subsequently confirmed with fluorescent bead injections (see below).

Cilia length is shortened in IFT morphants and oval mutant embryos

In order to manipulate cilia structure and assess their function in vivo, we cloned and disrupted the expression of zebrafish homologs of the IFT proteins of *polaris/IFT88/osm-5* and *hippi/IFT57/che-13*. The sequence homology and identity between human, mouse and zebrafish IFT genes are shown in Fig. S1 in the supplementary material. In addition, we analyzed the *oval* mutant (*ovl*^{tz288b}), which carries a point mutation in the zebrafish homolog of *polaris/IFT88/osm-5* leading to a protein truncation (L260X) (Tsujikawa and Malicki, 2004). The in situ expression of both *polaris(IFT88)* and *hippi(IFT57)* in 24-48 hpf embryos was ubiquitous with some enrichment along the pronephric ducts (see Fig. S2 in the supplementary material) and the brain ventricles, and also around KV (data not shown).

Using morpholino antisense oligonucleotides (MO), we disrupted protein function of the *hippi* and *polaris* genes. AUG and SP-morpholinos were designed for both genes. The effectiveness of SP-morpholinos was verified by RT-PCR using RNA from single embryos. The results show that morpholino suppression of mRNA splicing persists for at least 72 hours (Fig. 2O,P; see Fig. S5 in the supplementary material). Whole-mount immunostains for acetylated tubulin of 44 hpf. embryos

were performed and the specimens examined by confocal microscopy with extended focus. Wild-type pronephric tubules and ducts are ciliated along the entire length of the nephron. Individual cilia were visible in the posterior segment of the pronephric duct (Fig. 2A). In the pronephros of IFT morphant embryos and oval homozygous mutants, severe shortening or absence of cilia was observed along the entire length of the pronephric nephron, from the cloaca (Fig. 2B-D) to the anterior region of the pronephric tubules (data not shown). Cilia length was reduced from wild-type control 8.8±2.0 μm (n=107) to *polaris* MO 2.5±1.9 μm (n=271, P<0.001) and *hippi* MO 3.5±2.0 μm (n=141, P<0.001). In *oval* heterozygotes cilia were 10.0±2.5 μm (n=68) in length, while in *oval* homozygotes they were 3.7±2.1 μm (n=104, P<0.001). Ependymal cilia of the spinal central canal were similarly shortened or reduced in number in the morphant and mutant embryos (Fig. 2F-H) compared with wild-type controls (Fig. 2E). Length measurements of the cilia showed 2.1±0.7 μm (n=63) in wild type versus 0.9±0.5 μm (n=21, P<0.001) in *polaris* MO and 1.2±0.8 μm (n=46, P<0.001) in *hippi* MO. At the 8-10 somite stage KV cilia were also shortened or missing in IFT morphants compared with controls (Fig. 2I-K). When present, cilia length was 3.3±1.1 μm (n=119) in wild type versus 2.0±0.8 μm (n=25, P<0.001) in *polaris* MO and 1.4±0.6 μm (n=15, P<0.001) in *hippi* MO. In several instances cilia appeared largely absent in *hippi* MO embryos (Fig. 2K). Although reduced in length, pronephric cilia in IFT morphant or mutant embryos were comparable in structure and maintained a relatively normal 9+2 microtubule doublet ultrastructure (Fig. 2L-N).

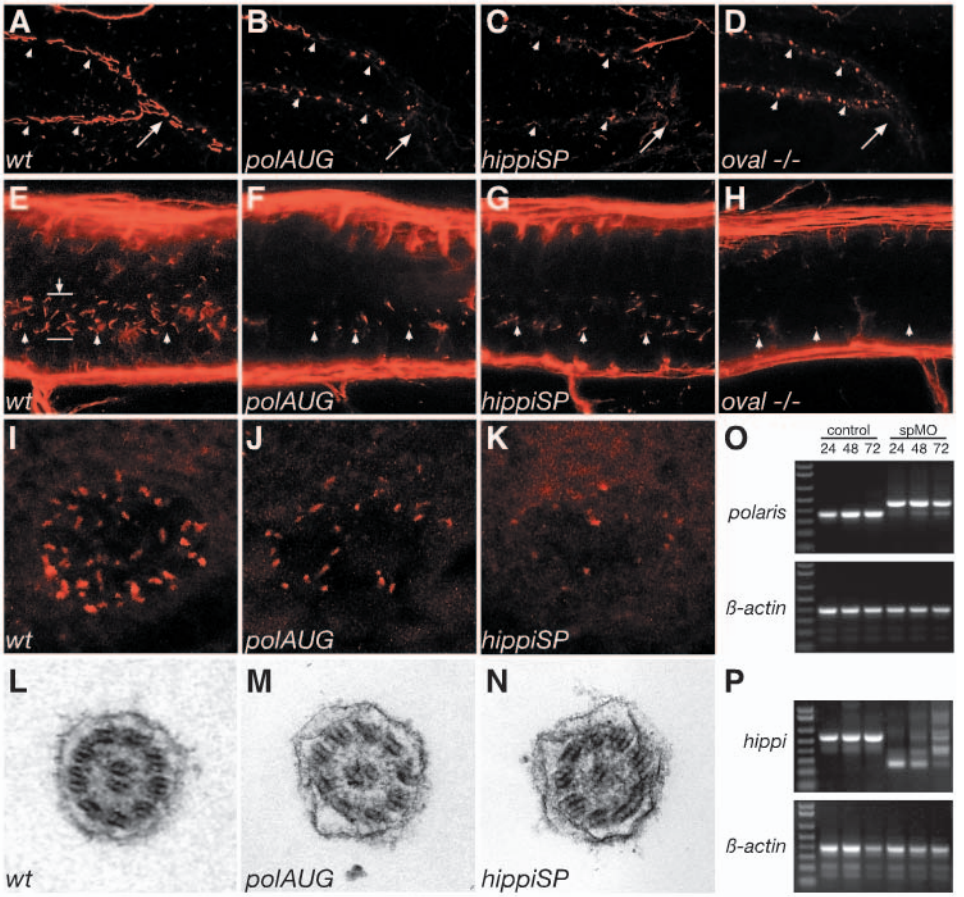

Fig. 2. Cilia structure is altered in IFT morphant embryos. A whole-mount confocal immunostaining of acetylated tubulin in 44 hpf embryos shows apical cilia in the pronephric ducts (A-D), the spinal canal (E-H) and Kupffer's vesicle (I-K). At 44 hpf *polaris* and *hippi* morphants (B,C), as well as *oval* homozygous mutant embryos (D), exhibit severely shortened cilia (arrowheads) compared with wild type (A). For reference, arrows in A-D indicate the point were the pronephric ducts merge at the cloaca. (E-H) Cilia (arrowheads) in the central canal (lumen indicated by arrow in E) of the spinal cord are also shortened or absent in *polaris* (F) and *hippi* (G) morphants and in *oval*$^{-/-}$ embryos (H) compared with wild type (E). Immunostaining of pronephros/central canal: anterior is to the left, dorsal to the top. Kupffer's vesicle cilia in *polaris* (J) and *hippi* (K) morphant embryos are greatly reduced compared with control (I). (L,M) Ultrastructure of the pronephric cilia in wild-type (L), *polaris* (M) and *hippi* (N) morphants show a typical 9+2 microtubule doublet pattern. (O) Molecular analysis of the effectiveness of SP-morpholinos inducing splice defects: RT-PCR of single embryos generates a 354 bp *polaris* fragment in control embryos, bridging part of exon 1 to part of exon 5 at 24, 48, 72 hpf (lane M, 1 Kb Plus DNA Ladder). *polaris*SP-injected embryos analyzed with the same primer sets at the same timepoints show a larger amplicon of 457 bp caused by a non-splicing of intron 2, which encodes a premature stop codon; the lower wild-type band recovers over time. Lower panel: RT-PCR of *β-actin* of the same RNA samples. (P) RT-PCR of *hippi* mRNA results in a 553 bp fragment in control embryos, whereas the amplicon is reduced in size in the *hippi*SP-treated embryos, indicating an in-frame deletion of exon 2 and 3 (lower band, 260 bp) or an out-of-frame deletion of exon 2 only (middle band, 378 bp); there is recovery of the wild-type band over time.

Cyst formation and hydrocephalus in IFT morphants and *oval*$^{-/-}$ embryos

To determine whether the previously described phenotypes associated with *IFT88/polaris* loss of function were also observed when expression of other IFT proteins was disrupted, we compared the phenotype of embryos injected with morpholinos targeting both *IFT88/polaris* and *IFT57/hippi*. Morpholinos targeting the translation start site (AUG) or the splice donor site (SP) of the second coding exon of *IFT88/polaris* or *IFT57/hippi* all led to pronephric cyst formation, hydrocephalus, ventrally curved body axis and pericardial edema in 72 hpf embryos (Fig. 3). Edema became generalized by day 5/6, when most of the embryos died. The kidney cyst and hydrocephalus were easily recognizable in the living fish, in which pigmentation was inhibited by PTU and also by histology (Fig. 3K). Body axis curvature, kidney cysts

and hydrocephalus were also observed in *oval* (*IFT88/polaris*) homozygous mutant embryos, confirming that the morpholino phenotypes we observed are due to *IFT88/polaris* loss of function (Fig. 3H) (Tsujikawa and Malicki, 2004).

The specificity of the morpholino was tested for the *hippi*AUG morpholino, for which an introduction of five mismatches completely abolished its effects (Fig. 3D). To further establish the specificity of the morpholino action, we performed rescue experiments for the *hippi*SP morpholino by co-injection of capped RNA made in vitro from zebrafish *hippi* cDNA. Zebrafish *hippi* mRNA injection alone did not cause an obvious phenotype; injected embryos appeared wild type. Co-injection of zebrafish *hippi* mRNA with morpholino completely rescued 36 out of 44 injected larvae to a wild-type-like phenotype; histological cross sections confirmed the absence of hydrocephalus and cyst formation in the co-injected larvae (see Fig. S3 in the supplementary material). Co-injected capped murine *hippi* RNA with *hippi*SP morpholino showed a complete rescue in 6 out of 26 embryos. Partial rescue was observed in 14 out of 26 embryos, with embryos showing a straight body axis and substantially reduced cyst formation. In 1 out of 26 doubly injected embryos, axis deformity and hydrocephalus were observed, but no cysts formed and the remaining five embryos did not show rescue (data not shown). The data demonstrate that the observed phenotypes are specific to loss of *IFT57/hippi* function and further suggest that *IFT57/hippi* protein function is in large part conserved in vertebrates.

Pronephric fluid flow is impaired in the IFT morphant/mutant embryos and can lead to cyst formation

The reduction in cilia length in IFT morphant embryos suggested that cilia motility might also be affected and contribute to the observed organ phenotypes. Indeed, in the IFT morphant embryos and *oval* homozygotes, moving cilia were rarely detected. The remaining motile cilia in these embryos appeared to be stumpy and had a faster, uncoordinated flickering movement (PolAUG 32.2±2.3 Hz, n=8, HippiSP 30.6±4.2 Hz, n=7, significantly different from control 20.0±3.2 Hz, n=34, P<0.001) (see Movie 6, Movie 5 in the supplementary material). The cloaca-directed, helical wave pattern of cilia beat observed in wild-type embryos was never seen in IFT morphant tubules or ducts.

To test if disturbed ciliary motility had an impact on fluid output from the pronephros, we performed dye excretion experiments. Tetramethylrhodamine-conjugated dextran (70 kD) injected into the common cardinal vein of living 3.5-day-old embryos was filtered in the glomerulus and excreted via the pronephric ducts at the cloaca (Fig. 4C). The time span after injection until the first visible urine excretion at the cloaca was 4.5±2.9 minutes (n=12) in wild-type

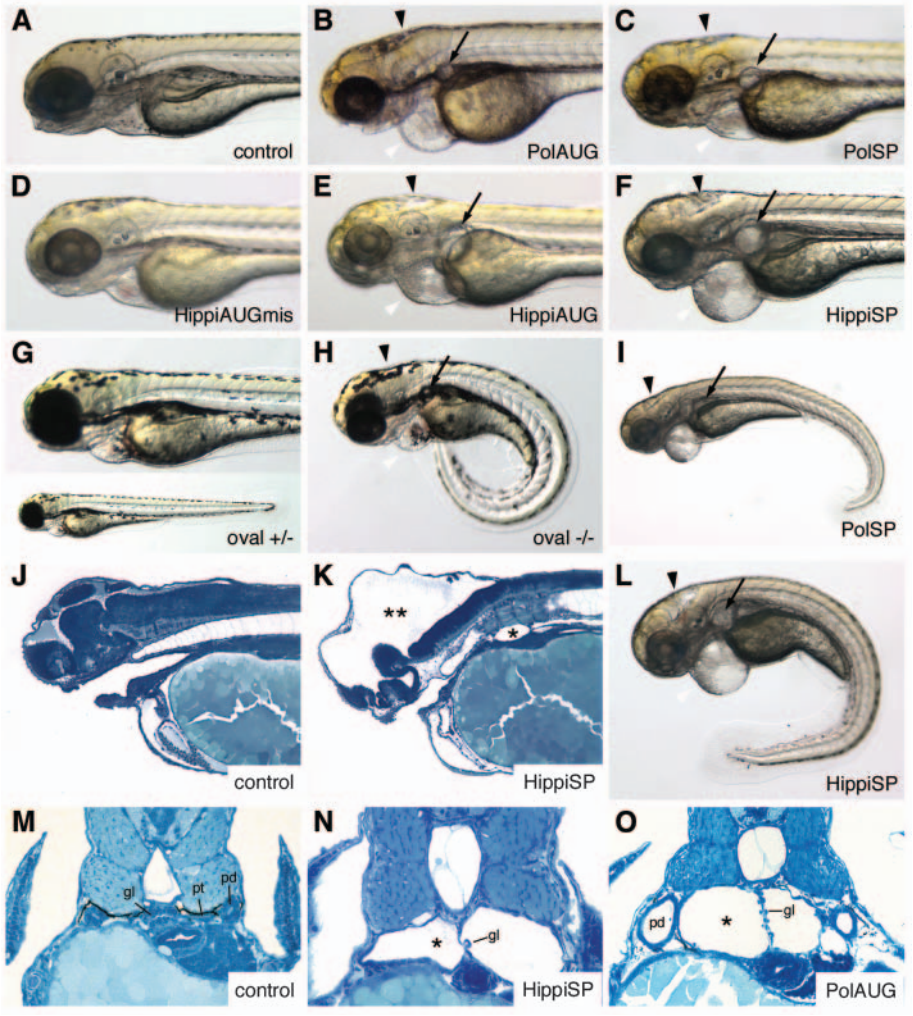

Fig. 3. IFT morphant phenotype: kidney cysts and hydrocephalus. Disruption of *polaris* function by injection of *polaris*AUG (B) and *polaris*SP (C,I) results in hydrocephalus (black arrowhead), pronephric cyst formation (arrow), pericardial edema (white arrowhead), and ventrally bent body axis at 72 hpf compared with non-injected control embryos (A). This phenotype imitates the *oval* homozygous mutant (H), in which the *polaris* gene is mutated. Heterozygous embryos are indistinguishable from wild-type controls (G). Embryos injected with the control *hippi*AUG mismatch morpholino have a normal morphology (D), whereas *hippi*AUG (E) and *hippi*SP (F) cause a phenotype similar to the *polaris* morphants and the *oval* homozygous mutant. (J) Wild-type embryo in longitudinal section. (K) *hippiSP* morphant embryo showing severe hydrocephalus (**) and kidney cyst (*). (L) *hippiSP* morphant embryo showing axis curvature, cysts (arrow) and hydrocephalus (arrowhead). (M) Histological cross sections of a 72 hpf control embryo show the midline fused glomerulus, pronephric tubules and pronephric ducts on either side. (N,O) *hippiSP* morphant embryos at 72 hpf show a cystic dilatation (*) of the pronephric tubules with a stretched glomerulus in the midline. (O) *polarisAUG* morphants show kidney cysts (*) and distension of the pronephric ducts. gl, glomerulus; pd, pronephric ducts; pt, pronephric tubules.

control embryos. A movie available in the supplemental data shows in fast motion how the fluorescent urine output is observed from 3-8 minutes post-injection (see Movie 3 in the supplementary material). In the morphant embryos, dye excretion fell to levels below our detection limits; no 'jet' of fluorescence at the cloaca was observed in 9 out of 9 *polaris*AUG and 9 out of 9 *hippi*SP morphants, even at timepoints more than 30 minutes post-injection (Fig. 4G,K), compared with a visible excretion in 22 out of 27 wild types. To demonstrate that the failure to detect fluorescent output was not because of blocked glomerular filtration, the embryos were sectioned and examined for dye passage and uptake by pronephric epithelial cells: all embryos showed endocytic uptake of the filtered dye by proximal duct cells, indicating that the fluorescent dextran was efficiently filtered in IFT morphant embryos (Fig. 4D,H,L). Similar to control wild-type embryos, *oval* heterozygotes showed dye excretion starting at 5.3±0.4 minutes (n=2) after injection. By contrast, two out of five oval homozygotes did not show dye excretion, and in the remaining three embryos, dye excretion was delayed, being first detectable at 13.7±5.5 minutes (n=3) (P=0.1, not significant) after injection, and the flow of excreted dye was markedly reduced. In these embryos, only the lumen of the common pronephric duct was visibly fluorescent (arrowhead), and there was no 'jet' of fluorescence in the medium outside the cloaca (arrow) (Fig. 4R). The data indicate that cilia function is required to maintain normal rates of fluid flow in the pronephros.

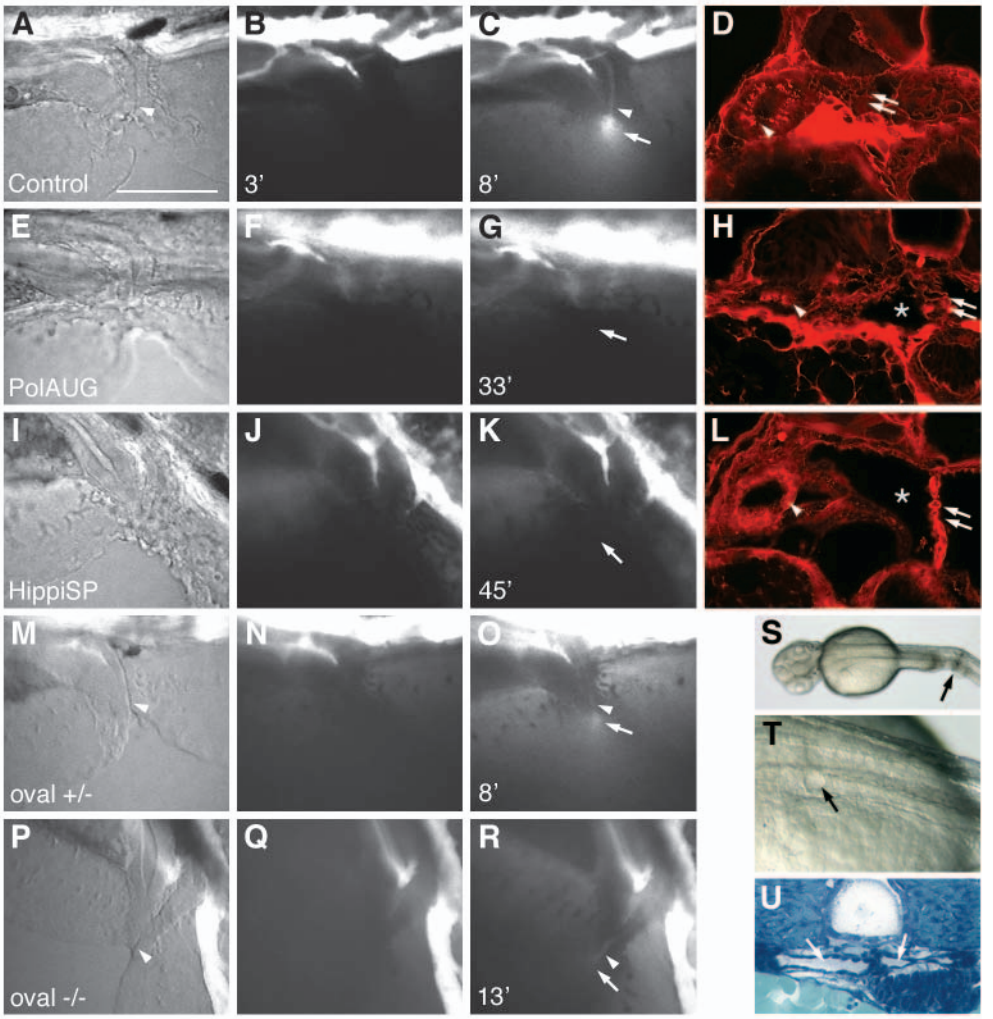

Fig. 4. Fluid flow is impaired by lack of normal cilia movement in the pronephros. Living embryos were injected with 5% tetramethylrhodamine-conjugated 70 k MW dextran into the circulation. After passage of the pronephric kidney, the dye was excreted at the cloaca (C, arrow). The images of the first column (A,E,I,M,P) are transmitted light images. The images in the second column (B,F,J,N,Q) were taken at 2-3 minutes post-injection, while the images in the third column (C,G,K,O,R) were captured when maximum excretion was reached. The time after injection that the image was captured is indicated in the bottom left of each panel. No fluorescent dye excretion via the cloaca was observed at timepoints >30 minutes in *polaris*AUG morphants (n=9) or *hippi*SP morphants (n=9), whereas in the control embryos excretion was observed in 22 individuals (n=27). On histology of the same embryos, all showed endocytic uptake of the dye in anterior duct cells (arrowhead) (D,H,L), indicating that the dye had been filtered via the glomerulus (double arrows) into the cyst lumens (*). In *oval* heterozygous embryos, excretion started at 5.3±0.4 seconds (n=2) (O), and 3 out of 5 *oval* homozygous embryos showed weak dye excretion at 13.7±5.5 seconds (n=3), whereas 2 did not show a visible output. In A-R anterior is to the left and dorsal is to the top. Mechanical obstruction of the pronephric ducts close to the cloaca (S, arrow) causes cystic distension of the anterior pronephric tubules within 30 minutes (T, arrow). The dilated tubules/glomerulus can be seen in cross sections (U, arrows). Scale bar: 100 µm.

To demonstrate that impaired fluid flow in the zebrafish pronephros could lead to cyst formation, we mechanically obstructed the pronephric ducts close to the cloaca (Fig. 4S). Number 5 Inox tweezers were used to pinch and physically obstruct the cloaca. This obstruction of fluid flow resulted in rapid pronephric cyst formation, within 30 minutes. Cystic distension of the pronephric tubules and the anterior segment of the pronephric ducts occurred well anterior to the point of occlusion. Cyst structure was verified in histological cross sections (Fig. 4T,U). Taken together with our data on disruption of cilia function, the results suggest that a reduction in flow rate in the pronephros may lead to back pressure at the site of fluid input to the pronephros and result in tubule luminal expansion and cyst formation.

Distension of the brain ventricles is associated with impaired fluid flow along the central canal of the spinal cord

To determine whether a similar loss of fluid flow could account for the distension of the brain ventricles seen in IFT morphant embryos, we injected 70 kD rhodamine-dextran into the fourth ventricle at the level of the hindbrain and labeled the cerebrospinal fluid in order to monitor its transport along the central canal of the spinal cord by fluorescence microscopy. The embryos were pretreated with BDM in order to prevent dye movement by an active circulation. The leading front of the dye traveling along the central canal was imaged at various timepoints and transport rate was quantified. In wild-type controls, the mean velocity of fluid movement in the spinal central canal was 27.0±1.9 μm/minute (n=4) (Fig. 5A,B), whereas it was reduced in the *polaris*AUG morphants to 11.3±3.3 μm/minute (n=5, P<0.001) (Fig. 5D) and in the *hippi*SP morphants to 12.0±1.7 μm/minute (n=3, P<0.001) (Fig. 5F). Identical results were obtained for the *oval* mutant (Fig. 5J). Impaired fluid flow probably results in fluid backup and distension of the brain ventricles and the development of hydrocephalus.

Disruption of dynein heavy chain 9 expression partially phenocopies the IFT-morphants

Previous studies of the role of cilia in kidney cystic disorders have suggested that kidney cilia are non-motile and act to sense fluid flow. Our results in zebrafish indicate that cilia motility is a primary factor in maintaining proper lumen size and kidney function. To distinguish between sensory versus motile cilia function, we sought to decrease cilia beat rate without causing gross changes in cilia length or structure. The outer doublet microtubules and associated dynein arms are critical for the initiation and propagation of ciliary bending, while the central pair/radial spokes system serves to regulate beat frequency and wave form (Smith and Yang, 2004). In order to disrupt cilia beat rate and pattern, we isolated an axonemal dynein heavy chain by RT-PCR using degenerate primers and RNA from isolated pronephric ducts of 72 hpf zebrafish larvae. A cDNA encoding the P1 domain, the primary ATP binding site that is essential for dynein motor function, of a dynein heavy chain homologous to human dynein heavy chain 9 (DYH9, AAF69004) was obtained. Injection of a morpholino (*dhc9*P1SP) targeting the splice donor site of the P1-domain coding exon resulted in mis-splicing of *dhc9* mRNA, producing either an out-of-frame deletion of the P1 ATP-binding domain or truncation after the P1 domain (see Fig. S5 in the supplementary material). The reduction of *dhc9* function partially phenocopied the IFT morphants/mutants (Fig. 6A) with injected embryos showing hydrocephalus and pericardial edema. Histological sectioning revealed distension of the pronephric tubules (Fig. 6G) and dilated pronephric ducts (Fig. 6H,I). The movement of the cilia in *dhc9*P1SP larvae was significantly slower than in wild-type control embryos: wild type 20.0±3.2 Hz (n=34) versus *dhc9*P1SP 14.7±3.9 Hz (n=15, P<0.001) (see Movie 7 in the supplementary material). The cilia beat frequency was also reduced in the central canal of the spinal cord with wild type 12.3±3.4 Hz (n=18) versus *dhc9*P1SP 7.3±1.9 Hz (n=6, P<0.001). The rate of dye transport in the spinal canal was also reduced in *dhc9*P1SP morphants (Fig. 6C) compared with wild type (Fig. 6B): wild type 27.0±1.9 μm/minute (n=7) versus *dhc9*P1SP 20.6±2.6 μm/minute (n=7, P<0.001). Excretion of circulating 70 kD rhodamine-dextran by the pronephros could be detected in only 5 out of 19 morphant embryos (Fig. 6L,M), and these embryos showed a delayed onset of 12.8±5.9 minutes (n=5) versus 4.5±2.9 minutes (n=12) in wild-type controls (P<0.01) (Fig. 6J,K). The embryos used for this experiment had sufficient circulation (circulating blood cells) despite pericardial edema. The data indicate that a reduction in beat frequency without changes in cilia structure is sufficient to cause the phenotypes associated with IFT protein loss of function.

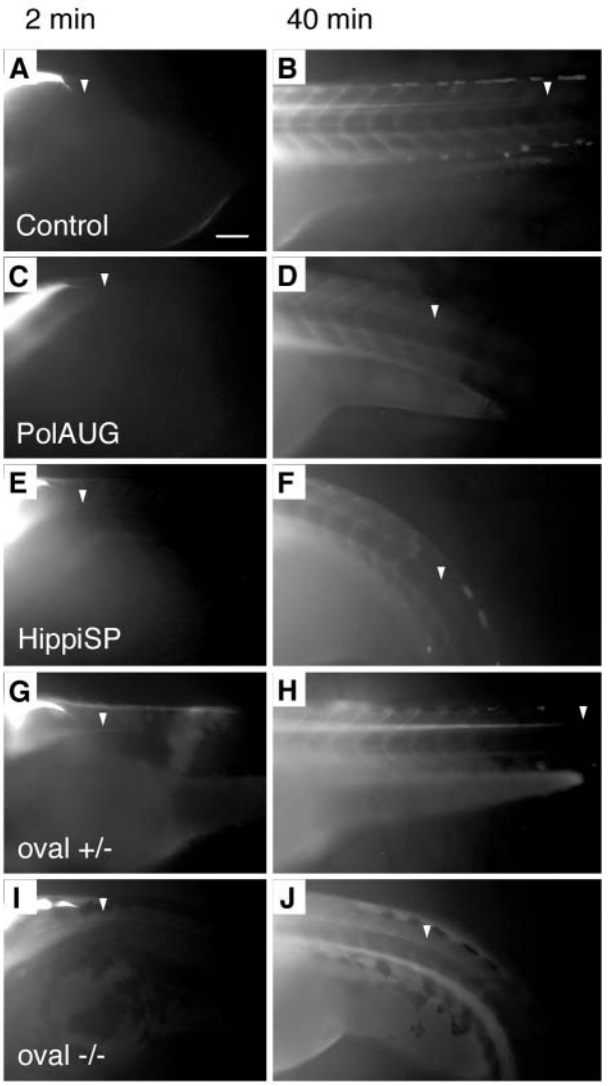

Fig. 5. Fluid flow is impaired by lack of normal cilia movement in the central canal of the spinal cord. BDM-pretreated embryos were injected with 5% tetramethylrhodamine-conjugated 70 k MW dextran into the fourth brain ventricle and dye distribution along the central canal of the spinal cord was recorded at various timepoints; shown are 2 and 40 minutes post-injection. Control (A,B) and *oval* heterozygous (G,H) show a distribution of the dye up to an anterior-posterior level of the tip of the yolk extension at 40 minutes (arrowheads) (B,H), whereas *polaris*AUG morphant (C,D), *hippi*SP morphant (E,F) and *oval* homozygotes (I,J) show reduced dye migration. Anterior to the left. Scale bar: 100 μm.

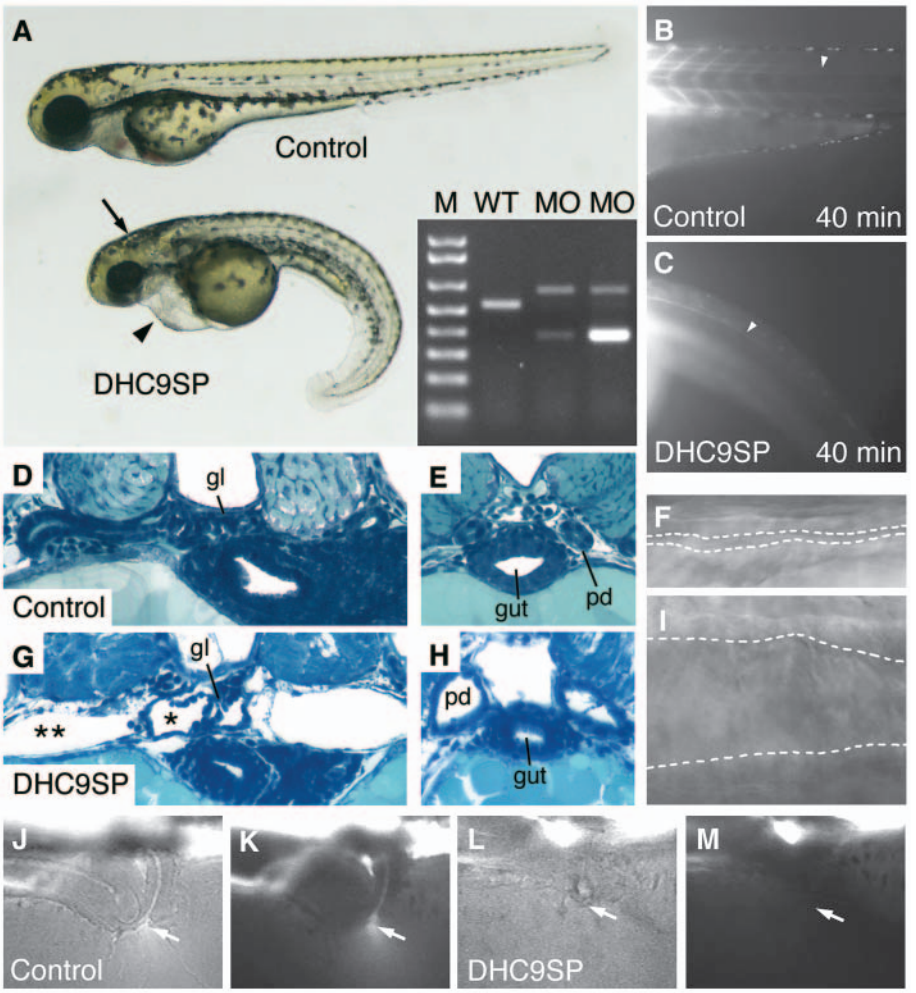

Fig. 6. Dynein heavy chain 9 knockdown morphants show abnormal cilia movements and phenotypic changes similar to the IFT morphants. A morpholino targeting the splice-donor site of the exon coding for the P1-domain of *dhc9* causes kidney cysts, hydrocephalus (arrow) and axis curvature (A). Sequencing RT-PCR of aberrant splice products (A, inset) revealed non-splicing of the adjacent intron with a premature stop codon (upper band) and an out-of-frame deletion of the P1-domain coding exon (lower band). The transport of injected fluorescent dye along the central canal of the spinal cord (B,C) is impaired in *dhc9*SP morphants (C) versus control (B). Histologically, *Dhc9*P1SP morphant embryos show distension of the tubules near the glomerulus (G) and dilated ducts (H) compared with wild-type control (D,E). The dilatation of the duct can also be seen in frames taken from Movie 7 (see supplementary material) (F, wild type; I, *Dhc9*P1SP morphant). (J-M) Dye excretion via the urine was not detected in *dhc9*SP morphants (arrows in L,M) versus control (J,K).

Impaired fluid flow in KV is associated with laterality defects

The presence of motile cilia in KV suggested that the fluid enclosed by the KV epithelium is 'stirred' and that, similar to the role of 'nodal flow' in the mouse, fluid movement might also play a role in establishing proper organ laterality in zebrafish. We visualized fluid movement in KV by injecting small fluorescent beads into the lumen of KV of 8-10 somite embryos. When viewed dorsally by videomicroscopy, injected beads moved in a counterclockwise direction (Fig. 7A-D, see Movie 10 in the supplementary material). Larger bead aggregates tended to collect in the center of KV, where they rotated in place in a counterclockwise direction. As noted above, cilia beating and the movement of small pieces of debris in KV was also in a counterclockwise direction (see Movie 9 in the supplementary material). To test whether fluid motion in KV required intact cilia, we examined injected bead movements in IFT88/*polaris* and IFT57*hippi* morphant embryos. The absence of normal cilia in KV of IFT morphant embryos completely abolished bead movement (Fig. 7E-H). The data indicate that counterclockwise cilia beating drives fluid in a counterclockwise flow pattern inside the confined space of KV.

It has been suggested that in order to achieve right-to-left fluid flow in the mouse node, only a portion of the circular cilia beat must be involved in fluid propulsion (Cartwright et al., 2004). If cilia were, for instance, tipped toward the posterior, then a cilium would extend into node fluid only on the right-to-left portion of the cycle. On the return left-to-right portion of stroke, the cilium would move close to the cell surface and produce only a small drag on node fluid. We therefore examined KV cilia by electron microscopy for signs that the cilia might be polarized in an anterior-posterior orientation. As shown in figure 7P, cilia and their associated basal bodies on the dorsal aspect ('roof') of KV were observed to be tipped to the posterior approximately 45° relative to the surface of the roof. We also observed that the cell membrane and cytoplasm adjacent to the cilium insertion appeared to be a site of active vesicle fusion (Fig. 7P).

To test whether loss of cilia-dependent fluid flow in KV resulted in laterality defects, we assayed expression of two conserved left-right genes, the nodal-related protein *southpaw* (*spaw*) and the bicoid-related transcription factor *pitx2*, which is downstream of *nodal*. At mid-somite stages (15-23) *southpaw* is expressed in the left lateral plate mesoderm (LPM) (Long et al., 2003). *pitx2* is also expressed in the same location at similar stages (Campione et al., 1999; Yan et al., 1999). Observed expression patterns for the IFT morphant embryos are shown in Fig. 7I-O. In IFT morphant embryos, right-sided or bilateral expression of *southpaw* was significantly increased, and in 33% of *polaris*AUG embryos *southpaw* expression was missing (Fig. 7R). Right-sided *pitx2* expression was increased in *polaris*AUG-injected embryos compared with wild type, and the frequency of absent signal was also increased. Significantly, *hippi*SP-injected embryos showed a complete absence of *pitx2*

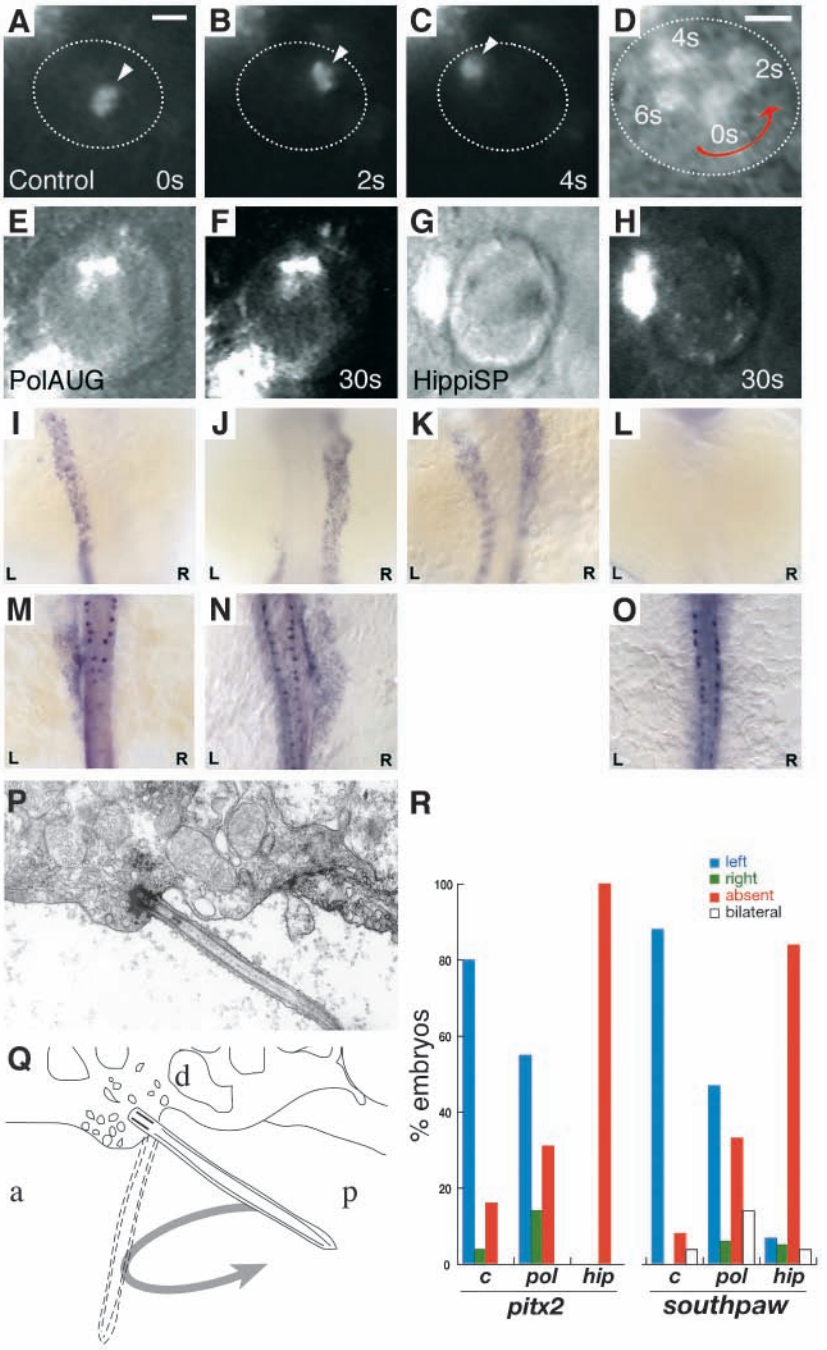

Fig. 7. Impaired fluid flow in Kupffer's vesicle is associated with defects in laterality. Embryos at the 8-10 somite stage were dechorionated and fluorescent beads were injected into Kupffer's vesicle. Control embryos showed a rotating movement of bead aggregates in a counterclockwise orientation (arrowheads in A-C) when viewed dorsally. Relative timepoints in seconds are indicated in the bottom right of each panel. The wall of Kupffer's vesicle is indicated by dotted lines. (D) Superposition and enlargement of frames (A-C) with an additional transmitted light frame showing the counterclockwise direction of movement. None of the injected morphant embryos (*polaris*AUG and *hippi*SP) showed this phenomenon (E-H). Abnormal expression of the laterality markers *pitx2* and *spaw* in *polaris*AUG and *hippi*SP embryos (I-O,R). In situ experiments were performed on 14-somite (*spaw*) and 20-somite (*pitx2*) embryos. Dorsal views of the lateral plate mesoderm are shown with the different expression patterns seen in *polaris*AUG embryos. *southpaw* was expressed on the left (I), right (J) or bilaterally (K), or in many cases absent (L). *pitx2* shows the same patterns (M, left-sided; N, right-sided; O, absent expression), with the exception of bilateral expression. Sagittal section electron micrograph (P) of the roof of Kupffer's vesicle showing, a single cilium and associated basal body. (Q) Diagram of the micrograph in P, detailing how the angle of the basal body [approximately 45° to the posterior (P)] would result in the cilium projecting into Kupffer's vesicle on the right-to-left portion of the counterclockwise rotary beat. (R) Frequency of laterality defects in *polaris* and *hippi* morphant embryos. Expression of *pitx2* and *southpaw* was randomized in *polaris*AUG embryos, while *hippi*SP embryos showed significantly higher numbers of embryos with no expression of *southpaw* and *pitx*2 (control, n=25; *polaris*AUG/*pitx2*, n=29; *polaris*AUG/*southpaw*, n=36; *hippi*SP/*pitx2*, n=40; *hippi*SP/*southpaw*, n=57). In embryos lacking laterality signals in the lateral plate mesoderm, gene expression was nevertheless maintained in the tailbud (*spaw*) and Rohon-Beard neurons (*pitx2*). Scale bar: 10 μm. a, anterior; d, dorsal.

expression and a near-complete absence of *southpaw* expression (Fig. 7R).

Discussion

The recent convergence of studies of kidney cystic disease, left-right asymmetry defects, retinal degeneration and flagella formation has led to the idea that defects in the formation or function of cilia may underlie pathologies observed in all these conditions. However, despite the focus on cilia as a central organelle in these phenotypes, it has been unclear what exactly cilia do to support normal organ development and function and how loss of this organelle can lead to such pathology. Our analysis of cilia during zebrafish organogenesis has demonstrated that cilia in the zebrafish pronephros, in the central canal of the spinal cord and in KV are motile. Beating cilia were found to induce fluid flow in all three organs. Lack of proper cilia formation due to inhibition of *IFT88/osm-5/polaris* or *IFT57/che-13/hippi* expression was associated with loss of fluid movement and resulted in pronephric cyst formation, left-right asymmetry defects and hydrocephalus. We conclude that back pressure from blocked flow and subsequent fluid accumulation may account for organ distension pathologies in the brain and kidney, while the loss of fluid flow in KV may result in absence of a mechanosensory signal regulating organ laterality.

Kidney cilia and cyst formation

Kidney cysts are the result of grossly expanded kidney tubule lumens. In human diseases such as autosomal dominant polycystic kidney disease, large numbers of cysts lead to kidney fibrosis and end-stage renal failure. A role for cilia in this disorder is implied from the variety of cilia-associated proteins that, when mutated, can cause tubules to become cystic (Barr et al., 2001; Blacque et al., 2004; Fan et al., 2004; Kim et al., 2004; Morgan et al., 2002; Murcia et al., 2000; Mykytyn et al., 2004; Otto et al., 2003; Pazour et al., 2000; Pazour et al., 2002; Qin et al., 2001; Sun et al., 2004; Taulman et al., 2001; Yoder et al., 2002). Cell culture studies of *PKD1* and *PKD2*, the genes responsible for autosomal dominant polycystic kidney disease, suggests that they act together in epithelial cells to mediate calcium entry upon flow-induced cilium deflection (Nauli et al., 2003; Praetorius and Spring, 2001). This model of cilia function proposes that the cilium acts as a passive sensor of tubule lumen mechanics and flow, providing a feedback signal that somehow limits lumen diameter. Our observation that zebrafish pronephric cilia are motile expands the repertoire of functions that kidney cilia can serve. Our results suggest that in more primitive kidneys, and perhaps at the earliest stages of kidney development, cilia can function as a motile 'fluid pump' to drive fluid through the nephron. Our results are consistent with an early report demonstrating that ciliated nephrons in the amphibian *Necturus* can generate hydrostatic pressures of up to 4.0-5.7 cm H_2O (White, 1929). In the elasmobranch (e.g. dogfish, skate) kidney, cells bearing multiple 9+2 cilia similar to those we describe in zebrafish, have been proposed to transport mucus secreted by duct cells and keep the ducts patent (Lacy et al., 1989).

Mammalian kidney cilia are not thought to be motile and instead are proposed to serve a sensory function. Nonetheless, some correspondence of our results to the metanephric kidney may be seen in the context of early mammalian development and human disease. In the human fetal kidney, bundles of 9+2 cilia have been observed in electron micrographs (Zimmermann, 1971) in kidney tubule lumens. Bundles of 9+2 cilia in the tubule lumen have also been observed in the adult human kidney under pathological conditions (Duffy and Suzuki, 1968; Hassan and Subramanyan, 1995; Katz and Morgan, 1984). Some primary cilia dyskinesia cases report an association between cilia motility dysfunction and cystic kidneys (Ibanez-Tallon et al., 2003) that, although rare, suggest that loss of cilia motility may also be important in some human cystic disorders. Obstruction of fluid flow has been identified as a cause of a specific type of human glomerular cyst formation occurring during fetal development (Potter, 1972; Woolf et al., 2004). One perspective that could take into account these observations in both fish and humans would be that the cilia that form first in early mammalian kidney development may be motile, recapitulating the cilia behavior we see in the more primitive fish pronephros. As development proceeds, cilia motility may be lost and cilia take on a new sensory function in the mature mammalian kidney. Implicit in this model is the idea that cyst formation, as a result of cilia dysfunction, could be caused by multiple mechanisms in fetal versus adult kidneys, and in pronephroi versus mature metanephroi. As more refined models of cystic gene defects are developed, e.g. conditional gene knockouts, these speculative ideas can be rigorously tested.

Increased cell proliferation has been also cited as a mechanism of cystic expansion in human disease (Nadasdy et al., 1995; Nauli et al., 2003) and as an initiating stimulus in some mouse models of cystic disease (MacRae Dell et al., 2004). Although cell proliferation could play a role in cyst expansion or progression in zebrafish, we have found no evidence of an increase in cell number in zebrafish cysts. Currently, a role for cell proliferation as an early, initiating event in cyst formation in mouse models of ADPKD (polycystin1 and polycystin2) and IFT mutants has yet to be established with quantitative data. It is likely that kidney cysts can arise from several different primary cellular defects, including increased proliferation, loss of cilia function and general cell dedifferention (reviewed by Arnaout, 2001). In this view, the initial stimulus for cyst formation may vary depending on the gene mutated.

In zebrafish, complete obstruction of the pronephric duct caused tubular distension within minutes, indicating that blocking fluid flow is sufficient for cyst formation. In IFT mutants/morphants it is likely that flow is reduced, but not completely blocked. Cyst formation in these larvae occurs more slowly over a period of hours after hatching. The *double bubble* pronephric cyst mutant, for instance, which we have recently found to be defective in cilia formation (T. Obara and I.A.D., unpublished), has a patent pronephric duct lumen based on serial sectioning, and forms cysts between 2 and 2.5 dpf (Drummond et al., 1998). Also, while the excretion rate in IFT morphants and oval homozygotes was not sufficient to generate a jet of fluorescent urine, dye fluorescence was visible in the common pronephric duct lumen, indicating that the duct remains unobstructed. It is striking that complete obstruction initiates cyst formation only in the anterior pronephric tubules and not, for instance, along the length of the pronephric duct. The anterior pronephric tubules and glomerulus is also the initial site of cyst formation in all zebrafish cyst mutants reported (Drummond et al., 1998; Sun et al., 2004). Only several hours after initial anterior cyst formation is observed does the duct lumen begin to expand, for instance as we report here for the *dhc9* morphant. It is possible that the anterior tubule/glomerulus may be the most labile structure in the forming pronephros at the time when voluminous fluid flow begins (at hatching?) and thus most distensible by fluid pressure. It is notable that many zebrafish cyst mutants show a curled body axis (Drummond et al., 1998; Sun et al., 2004). It is unlikely that the reduction in flow/cyst formation we observe is a secondary consequence of body curvature, because many mutants exist with ventral axis curvature that do not develop cysts in the kidney, and initiation of cyst formation occurs prior to the development of axis curvature (Drummond et al., 1998).

Motile cilia in the brain and hydrocephalus

Retention of cerebrospinal fluid in the brain ventricles by malabsorption or impaired drainage causes a distension of the brain ventricles or hydrocephalus. Our results demonstrate that motile cilia in the spinal canal are necessary to maintain normal cerebrospinal fluid distribution and that impaired fluid flow results in a backup of fluid in the central canal and brain ventricles. Our results are consistent with previous observations that human ependymal cilia are motile (Worthington and Cathcart, 1963; Worthington and Cathcart, 1966). In addition, patients with PCD suffer from

hydrocephalus in addition to respiratory syndromes associated with loss of lung cilia function. Mice with mutations in *mdnah5*, *hfh4* and *polaris* (*IFT88/tg737*) (Ibanez-Tallon et al., 2003) all exhibit hydrocephalus. While our work was in review, Ibanez-Tallon and co-workers demonstrated that in mouse *mdnah5* mutants the movement of beads injected into the brain ventricle was impaired, further implying a role for motile cilia in the hydrocephalus seen in these animals (Ibanez-Tallon et al., 2004). Although additional driving forces for fluid flow along the central canal may exist (for instance, fluid secretion and reabsorption), motile cilia appear to be crucial for normal cerebrospinal fluid flow rates.

The 9+0 cilia are thought to be immotile as they lack the central microtubule pair normally associated with motile cilia. Ependymal cilia in zebrafish have a 9+0 axonemal microtubular pattern and yet are motile, indicating that the presence of a central microtubule pair is not a prerequisite for motility. This is similar to the mouse node, where 9+0 cilia beat in a rotary fashion (Nonaka et al., 2002). The presence of dynein arms on the outer microtubule pairs may be a better predictor of whether a cilium is sensory (immotile) or motile. A central pair in 9+2 cilia may have more relevance to the cilia wave form. The beat pattern of 9+2 cilia has been described as a planar waveform (O'Callaghan et al., 1999; Shimizu and Koto, 1992; Smith and Yang, 2004). Zebrafish ependymal cilia and mouse node cilia beat in a simpler rotary pattern (McGrath et al., 2003).

Motile cilia in KV and laterality defects

Previous work in the mouse has demonstrated that cilia function and nodal flow are required in the establishment of left-right asymmetry (Bisgrove et al., 2003; Hamada et al., 2002). The ciliated epithelium of the mouse ventral node has been shown to cause fluid flow in a right-to-left direction across its surface (Nonaka et al., 1998; Sulik et al., 1994). The direction of this fluid flow seems to be crucial, as inverting the direction causes situs inversus, and no flow causes randomization of the left right axis (Nonaka et al., 2002). Fluid flow may also be important in determining situs in humans, as evidenced by the random organ situs seen in patients suffering from PCD, in which cilia motility is impaired (Afzelius, 1985; Ibanez-Tallon et al., 2003). In zebrafish and other teleosts, KV is the functional equivalent of the mouse node (Brummett and Dumont, 1978; Essner et al., 2002). Early morphological studies in *Fundulus heteroclitus* showed clearly that the cells of the dorsal 'roof' of KV are uniformly ciliated (Brummett and Dumont, 1978). Support for a role for KV in left-right axis determination was demonstrated recently by the finding that the T-box transcription factor *no tail* is required for the morphogenesis of KV and *no tail* mutant embryos exhibit randomized left-right axes (Amack and Yost, 2004). Importantly, selective suppression of no tail function in the dorsal forerunner cells, the progenitors of KV, specifically inhibits KV development in the absence of other embryonic defects and leads to randomization of the left-right axis (Amack and Yost, 2004). We show that, like the mouse node, the zebrafish KV is a ciliated structure and a site of dynamic cilia-driven fluid flow. We observe that flow occurs in a circular, counterclockwise direction. However, some aspects of our data would also suggest that the primary propulsive force is in a right-to-left direction, similar to the mouse node. First, cilia anchored in the roof of KV are tipped toward the posterior. As suggested by previous modeling studies (Cartwright et al., 2004), cilia beating in a counterclockwise direction at this angle would be predicted to extend into KV fluid on the right-to-left stroke and pass along the cell surface on the return left-to-right stroke. The predicted result of this beat pattern would be active propulsion in the right-to-left (extended) stroke and substantially less propulsion as the cilium glides over the cell surface. In addition to the ultrastructural evidence, support for this idea can be seen in the movies of KV bead-injected embryos, where bead movement appears to be faster in the right-to-left direction. In Movie 10 (in the supplementary material), the bead aggregate makes four trips around the periphery of KV. The average time for right-to-left transit (2.6±0.13 s.e.m. seconds) is significantly less than for left-to-right transit (3.8±0.15 s.e.m. seconds). While it is clear that more detailed quantitative studies will be required to extrapolate on these observations, the results suggest that KV fluid may be driven in a right-to-left direction; the left-to-right movement completing the circular pattern may be passive return flow. A passive return flow might also be expected to occur in vivo in the mouse node (Cartwright et al., 2004). This is because the node in mouse is also a closed structure, i.e. the ciliated node surface is covered and enclosed by Reichert's membrane in the embryo (Nonaka et al., 1998). In most flow studies to date, Reichert's membrane is first removed to gain access to the node surface (Nonaka et al., 1998).

Two hypotheses have been put forward to suggest a mechanism implicating fluid flow in left-right axis determination. In simple terms, the alternatives are that: (1) a morphogen gradient is established by right-to-left fluid flow (Nonaka et al., 1998; Okada et al., 1999); or (2) fluid flow per se is sufficient to provide a mechanical signal that breaks left-right symmetry, possibly by stimulating non-motile, mechanosensory cilia and subsequent intracellular calcium signaling (McGrath et al., 2003; Tabin and Vogan, 2003). Given that the KV is a closed vesicle and fluid flow inside the vesicle is circular, it seems unlikely that the role of fluid flow would be to drive a morphogen to one side of the zebrafish embryo, although models for such an effect of cilia have been proposed (Cartwright et al., 2004). In our view it is more likely that counterclockwise fluid flow is sensed to generate an asymmetric signal; however, at present the underlying mechanisms are unknown. We have also observed laterality defects in *polycystin2* knockdown zebrafish embryos (Obara et al., unpublished), similar to that seen in the mouse. *polycystin2*, as a member of the TRP mechanosensory ion channels, may play a role in transducing KV fluid flow in the zebrafish.

Our results are consistent with the idea that cilia in the KV fulfill a function analogous to cilia in the node region of mouse, i.e. they generate a leftward flow that induces left-side specific gene expression. However, because IFT proteins and cilia have also been implicated in other processes (Huangfu et al., 2003; Tsujikawa and Malicki, 2004), it cannot be formally excluded that the left-right defects are caused by mechanisms unrelated to nodal flow. For example, in the mouse, IFT proteins have been implicated in hedgehog signaling (Huangfu et al., 2003), and hedgehog signaling has been implicated in left-right patterning (Zhang et al., 2001). Hence, some IFT mutants might affect left-right development by disrupting hedgehog signaling in the mouse. This scenario is less likely in zebrafish,

because loss of hedgehog signaling does not lead to left-right defects (Chen et al., 2001). The widespread expression of IFT genes in early embryos also leaves open the possibility that IFTs could function in dorsal forerunners or other cells and tissues that form before KV. As our experiments do not identify the stage at which IFT proteins act in the process of establishing left-right asymmetry, we cannot rule out a role for *hippi* or *polaris* prior to the formation of KV. Loss of IFT function could conceivably have additional effects on KV-associated gene expression that precedes left-sided *southpaw* expression and that could influence the competence of KV to generate a left-sided signal. While we have not ruled this out, the observation that in IFT morphants, *southpaw* and *pitx2* expression was not affected in tissues other than the lateral plate mesoderm indicates that loss of IFT function does not have widespread effects on the expression of these two markers. It is reasonable to expect that multiple, redundant mechanisms may act to establish left-right asymmetry, some of which may function to maintain, propagate or amplify other signaling systems. At present, we favor a direct role of IFT proteins and cilia in left-right patterning by generating flow in KV as one such signaling system that is now amenable to experimental manipulation in the zebrafish.

In summary, by analyzing the phenotypes of zebrafish IFT protein morpholino knockdowns and an *IFT88* point mutant (*oval*), and by disrupting expression of a dynein heavy chain, we show that cilia-driven fluid flow is crucial for the early development of zebrafish embryos. Fluid flow in KV correlates with determination of the left-right axis and its impairment causes laterality defects. Compromised fluid flow along the central canal of the spinal cord correlates with backup of fluid in the brain ventricles, leading to hydrocephalus. In the pronephros, cilia motility is required for high rates of flow. Disruption of pronephric fluid flow leads to cyst formation in zebrafish. These results should serve to refocus attention on biological fluid dynamics as one common mechanism underlying various disorders of epithelial tissue structure and function.

The authors would like to thank members of the Drummond lab, Stephanie Wiessner, Jinhua Zhao, Tomoko Obara and Narendra Pathak, for the helpful discussions and support. We also thank Dr Jarema Malicki for providing the *oval* mutant; Mary McKee and Dennis Brown for assistance with electron microscopy; Dirk Hentschel for contributing to the development of dextran injection methods; Richard Bouley, Valerie and Nicolas DaSilva of the MGH Membrane Biology Group for helpful discussions; Margaret Boulos, Humberto Urquiza, Amy Doherty, Marcellino Pina and Eric Stone for aquaculture support; and the other members of the Developmental Biology Lab at the Massachusetts General Hospital for critical input into this work. Genomic sequence used in this work was produced by the Zebrafish Sequencing Group at the Sanger Institute and can be obtained from ftp://ftp.ensembl.org/pub/traces/zebrafish.

This work was supported by NIDDK grants DK53093 and DK54711 to I.A.D., DK65655 to B.K.Y. and NIH 5RO1 GM56211 to A.F.S. A.F.S. is an Irma T. Hirschl Trust Career Scientist and an Established Investigator of the American Heart Association. C.J.H. is supported through a T32 training grant (DK07545) to Dr D. Benos.

Supplementary material

Supplementary material for this article is available at
http://dev.biologists.org/cgi/content/full/132/8/1907/DC1

References

Afzelius, B. A. (1985). The immotile-cilia syndrome: a microtubule-associated defect. *CRC Crit. Rev. Biochem.* **19**, 63-87.

Amack, J. D. and Yost, H. J. (2004). The T box transcription factor no tail in ciliated cells controls zebrafish left-right asymmetry. *Curr. Biol.* **14**, 685-690.

Arnaout, M. A. (2001). Molecular genetics and pathogenesis of autosomal dominant polysyctic kidney disease. *Ann. Rev. Med.* **52**, 93-123.

Barr, M. M., DeModena, J., Braun, D., Nguyen, C. Q., Hall, D. H. and Sternberg, P. W. (2001). The Caenorhabditis elegans autosomal dominant polycystic kidney disease gene homologs lov-1 and pkd-2 act in the same pathway. *Curr. Biol.* **11**, 1341-1346.

Bisgrove, B. W., Morelli, S. H. and Yost, H. J. (2003). Genetics of human laterality disorders: insights from vertebrate model systems. *Annu. Rev. Genomics Hum. Genet.* **4**, 1-32.

Blacque, O. E., Reardon, M. J., Li, C., McCarthy, J., Mahjoub, M. R., Ansley, S. J., Badano, J. L., Mah, A. K., Beales, P. L., Davidson, W. S. et al. (2004). Loss of C. elegans BBS-7 and BBS-8 protein function results in cilia defects and compromised intraflagellar transport. *Genes Dev.* **18**, 1630-1642.

Brody, S. L., Yan, X. H., Wuerffel, M. K., Song, S. K. and Shapiro, S. D. (2000). Ciliogenesis and left-right axis defects in forkhead factor HFH-4-null mice. *Am. J. Respir. Cell. Mol. Biol.* **23**, 45-51.

Brummett, A. R. and Dumont, J. N. (1978). Kupffer's vesicle in Fundulus heteroclitus: a scanning and transmission electron microscope study. *Tissue Cell* **10**, 11-22.

Campione, M., Steinbeisser, H., Schweickert, A., Deissler, K., van Bebber, F., Lowe, L. A., Nowotschin, S., Viebahn, C., Haffter, P., Kuehn, M. R. et al. (1999). The homeobox gene Pitx2: mediator of asymmetric left-right signaling in vertebrate heart and gut looping. *Development* **126**, 1225-1234.

Cano, D. A., Murcia, N. S., Pazour, G. J. and Hebrok, M. (2004). orpk mouse model of polycystic kidney disease reveals essential role of primary cilia in pancreatic tissue organization. *Development* **131**, 3457-3467.

Cartwright, J. H., Piro, O. and Tuval, I. (2004). Fluid-dynamical basis of the embryonic development of left-right asymmetry in vertebrates. *Proc. Natl. Acad. Sci. USA* **101**, 7234-7239.

Chen, W., Burgess, S. and Hopkins, N. (2001). Analysis of the zebrafish smoothened mutant reveals conserved and divergent functions of hedgehog activity. *Development* **128**, 2385-2396.

Chen, J., Knowles, H. J., Hebert, J. L. and Hackett, B. P. (1998). Mutation of the mouse hepatocyte nuclear factor/forkhead homologue 4 gene results in an absence of cilia and random left-right asymmetry. *J. Clin. Invest.* **102**, 1077-1082.

Drummond, I. A., Majumdar, A., Hentschel, H., Elger, M., Solnica-Krezel, L., Schier, A. F., Neuhauss, S. C., Stemple, D. L., Zwartkruis, F., Rangini, Z. et al. (1998). Early development of the zebrafish pronephros and analysis of mutations affecting pronephric function. *Development* **125**, 4655-4667.

Duffy, J. L. and Suzuki, Y. (1968). Ciliated human renal proximal tubular cells. Observations in three cases of hypercalcemia. *Am. J. Pathol.* **53**, 609-616.

Essner, J. J., Vogan, K. J., Wagner, M. K., Tabin, C. J., Yost, H. J. and Brueckner, M. (2002). Conserved function for embryonic nodal cilia. *Nature* **418**, 37-38.

Fan, Y., Esmail, M. A., Ansley, S. J., Blacque, O. E., Boroevich, K., Ross, A. J., Moore, S. J., Badano, J. L., May-Simera, H., Compton, D. S. et al. (2004). Mutations in a member of the Ras superfamily of small GTP-binding proteins causes Bardet-Biedl syndrome. *Nat. Genet.* **36**, 989-993.

Hamada, H., Meno, C., Watanabe, D. and Saijoh, Y. (2002). Establishment of vertebrate left-right asymmetry. *Nat. Rev. Genet.* **3**, 103-113.

Hassan, M. O. and Subramanyan, S. (1995). Ciliated renal tubular cells in crescentic glomerulonephritis. *Ultrastruct. Pathol.* **19**, 201-203.

Hou, X., Mrug, M., Yoder, B. K., Lefkowitz, E. J., Kremmidiotis, G., D'Eustachio, P., Beier, D. R. and Guay-Woodford, L. M. (2002). Cystin, a novel cilia-associated protein, is disrupted in the cpk mouse model of polycystic kidney disease. *J. Clin. Invest.* **109**, 533-540.

Huangfu, D., Liu, A., Rakeman, A. S., Murcia, N. S., Niswander, L. and Anderson, K. V. (2003). Hedgehog signalling in the mouse requires intraflagellar transport proteins. *Nature* **426**, 83-87.

Humphrey, C. D. and Pittman, F. E. (1974). A simple methylene blue-azure II-basic fuchsin stain for epoxy-embedded tissue sections. *Stain Technol.* **49**, 9-14.

Ibanez-Tallon, I., Heintz, N. and Omran, H. (2003). To beat or not to beat:

roles of cilia in development and disease. *Hum. Mol. Genet.* **12 Spec No 1**, R27-R35.

Ibanez-Tallon, I., Pagenstecher, A., Fliegauf, M., Olbrich, H., Kispert, A., Ketelsen, U. P., North, A., Heintz, N. and Omran, H. (2004). Dysfunction of axonemal dynein heavy chain Mdnah5 inhibits ependymal flow and reveals a novel mechanism for hydrocephalus formation. *Hum. Mol. Genet.* **13**, 2133-2141.

Igarashi, P. and Somlo, S. (2002). Genetics and pathogenesis of polycystic kidney disease. *J. Am. Soc. Nephrol.* **13**, 2384-2398.

Katz, S. M. and Morgan, J. J. (1984). Cilia in the human kidney. *Ultrastruct. Pathol.* **6**, 285-294.

Kim, J. C., Badano, J. L., Sibold, S., Esmail, M. A., Hill, J., Hoskins, B. E., Leitch, C. C., Venner, K., Ansley, S. J., Ross, A. J. et al. (2004). The Bardet-Biedl protein BBS4 targets cargo to the pericentriolar region and is required for microtubule anchoring and cell cycle progression. *Nat. Genet.* **36**, 462-470.

Lacy, E. R., Luciano, L. and Reale, E. (1989). Flagellar cells and ciliary cells in the renal tubule of elasmobranchs. *J. Exp. Zool.* **Suppl. 2**, 186-192.

Layton, W. M., Jr (1976). Random determination of a developmental process: reversal of normal visceral asymmetry in the mouse. *J. Hered.* **67**, 336-338.

Long, S., Ahmad, N. and Rebagliati, M. (2003). The zebrafish nodal-related gene southpaw is required for visceral and diencephalic left-right asymmetry. *Development* **130**, 2303-2316.

Lowe, L. A., Supp, D. M., Sampath, K., Yokoyama, T., Wright, C. V., Potter, S. S., Overbeek, P. and Kuehn, M. R. (1996). Conserved left-right asymmetry of nodal expression and alterations in murine situs inversus. *Nature* **381**, 158-161.

MacRae Dell, K., Nemo, R., Sweeney, W. E., Jr and Avner, E. D. (2004). EGF-related growth factors in the pathogenesis of murine ARPKD. *Kidney Int.* **65**, 2018-2029.

Marszalek, J. R., Ruiz-Lozano, P., Roberts, E., Chien, K. R. and Goldstein, L. S. (1999). Situs inversus and embryonic ciliary morphogenesis defects in mouse mutants lacking the KIF3A subunit of kinesin-II. *Proc. Natl. Acad. Sci. USA* **96**, 5043-5048.

McGrath, J., Somlo, S., Makova, S., Tian, X. and Brueckner, M. (2003). Two populations of node monocilia initiate left-right asymmetry in the mouse. *Cell* **114**, 61-73.

Morgan, D., Goodship, J., Essner, J. J., Vogan, K. J., Turnpenny, L., Yost, J., Tabin, C. J. and Strachan, T. (2002). The left-right determinant inversin has highly conserved ankyrin repeat and IQ domains and interacts with calmodulin. *Hum. Genet.* **110**, 377-384.

Moyer, J. H., Lee-Tischler, M. J., Kwon, H. Y., Schrick, J. J., Avner, E. D., Sweeney, W. E., Godfrey, V. L., Cacheiro, N. L., Wilkinson, J. E. and Woychik, R. P. (1994). Candidate gene associated with a mutation causing recessive polycystic kidney disease in mice. *Science* **264**, 1329-1333.

Murcia, N. S., Richards, W. G., Yoder, B. K., Mucenski, M. L., Dunlap, J. R. and Woychik, R. P. (2000). The Oak Ridge Polycystic Kidney (orpk) disease gene is required for left-right axis determination. *Development* **127**, 2347-2355.

Mykytyn, K., Mullins, R. F., Andrews, M., Chiang, A. P., Swiderski, R. E., Yang, B., Braun, T., Casavant, T., Stone, E. M. and Sheffield, V. C. (2004). Bardet-Biedl syndrome type 4 (BBS4)-null mice implicate Bbs4 in flagella formation but not global cilia assembly. *Proc. Natl. Acad. Sci. USA* **101**, 8664-8669.

Nadasdy, T., Laszik, Z., Lajoie, G., Blick, K. E., Wheeler, D. E. and Silva, F. G. (1995). Proliferative activity of cyst epithelium in human renal cystic diseases. *J. Am. Soc. Nephrol.* **5**, 1462-1468.

Nauli, S. M. and Zhou, J. (2004). Polycystins and mechanosensation in renal and nodal cilia. *BioEssays* **26**, 844-856.

Nauli, S. M., Alenghat, F. J., Luo, Y., Williams, E., Vassilev, P., Li, X., Elia, A. E., Lu, W., Brown, E. M., Quinn, S. J. et al. (2003). Polycystins 1 and 2 mediate mechanosensation in the primary cilium of kidney cells. *Nat. Genet.* **33**, 129-137.

Nonaka, S., Shiratori, H., Saijoh, Y. and Hamada, H. (2002). Determination of left-right patterning of the mouse embryo by artificial nodal flow. *Nature* **418**, 96-99.

Nonaka, S., Tanaka, Y., Okada, Y., Takeda, S., Harada, A., Kanai, Y., Kido, M. and Hirokawa, N. (1998). Randomization of left-right asymmetry due to loss of nodal cilia generating leftward flow of extraembryonic fluid in mice lacking KIF3B motor protein. *Cell* **95**, 829-837.

O'Callaghan, C., Sikand, K. and Rutman, A. (1999). Respiratory and brain ependymal ciliary function. *Pediatr. Res.* **46**, 704-707.

Okada, Y., Nonaka, S., Tanaka, Y., Saijoh, Y., Hamada, H. and Hirokawa, N. (1999). Abnormal nodal flow precedes situs inversus in iv and inv mice. *Mol. Cell* **4**, 459-468.

Otto, E. A., Schermer, B., Obara, T., O'Toole, J. F., Hiller, K. S., Mueller, A. M., Ruf, R. G., Hoefele, J., Beekmann, F., Landau, D. et al. (2003). Mutations in INVS encoding inversin cause nephronophthisis type 2, linking renal cystic disease to the function of primary cilia and left-right axis determination. *Nat. Genet.* **34**, 413-420.

Pazour, G. J. and Witman, G. B. (2003). The vertebrate primary cilium is a sensory organelle. *Curr. Opin. Cell Biol.* **15**, 105-110.

Pazour, G. J., Dickert, B. L., Vucica, Y., Seeley, E. S., Rosenbaum, J. L., Witman, G. B. and Cole, D. G. (2000). Chlamydomonas IFT88 and its mouse homologue, polycystic kidney disease gene tg737, are required for assembly of cilia and flagella. *J. Cell Biol.* **151**, 709-718.

Pazour, G. J., San Agustin, J. T., Follit, J. A., Rosenbaum, J. L. and Witman, G. B. (2002). Polycystin-2 localizes to kidney cilia and the ciliary level is elevated in orpk mice with polycystic kidney disease. *Curr. Biol.* **12**, R378-R380.

Perkins, L. A., Hedgecock, E. M., Thomson, J. N. and Culotti, J. G. (1986). Mutant sensory cilia in the nematode Caenorhabditis elegans. *Dev. Biol.* **117**, 456-487.

Piperno, G. and Fuller, M. T. (1985). Monoclonal antibodies specific for an acetylated form of alpha-tubulin recognize the antigen in cilia and flagella from a variety of organisms. *J. Cell Biol.* **101**, 2085-2094.

Potter, E. L. (1972). *Normal and Abnormal Development of the Kidney*. Chicago: Year Book Medical Publishers.

Praetorius, H. A. and Spring, K. R. (2001). Bending the MDCK cell primary cilium increases intracellular calcium. *J. Membr. Biol.* **184**, 71-79.

Qin, H., Rosenbaum, J. L. and Barr, M. M. (2001). An autosomal recessive polycystic kidney disease gene homolog is involved in intraflagellar transport in C. elegans ciliated sensory neurons. *Curr. Biol.* **11**, 457-461.

Richards, W. G., Yoder, B. K., Isfort, R. J., Detilleux, P. G., Foster, C., Neilsen, N., Woychik, R. P. and Wilkinson, J. E. (1996). Oval cell proliferation associated with the murine insertional mutation TgN737Rpw. *Am. J. Pathol.* **149**, 1919-1930.

Rosenbaum, J. L. and Witman, G. B. (2002). Intraflagellar transport. *Nat. Rev. Mol. Cell. Biol.* **3**, 813-825.

Shimizu, A. and Koto, M. (1992). Ultrastructure and movement of the ependymal and tracheal cilia in congenitally hydrocephalic WIC-Hyd rats. *Childs Nerv. Syst.* **8**, 25-32.

Smith, E. F. and Yang, P. (2004). The radial spokes and central apparatus: mechano-chemical transducers that regulate flagellar motility. *Cell Motil. Cytoskeleton* **57**, 8-17.

Sulik, K., Dehart, D. B., Iangaki, T., Carson, J. L., Vrablic, T., Gesteland, K. and Schoenwolf, G. C. (1994). Morphogenesis of the murine node and notochordal plate. *Dev. Dyn.* **201**, 260-278.

Sun, Z., Amsterdam, A., Pazour, G. J., Cole, D. G., Miller, M. S. and Hopkins, N. (2004). A genetic screen in zebrafish identifies cilia genes as a principal cause of cystic kidney. *Development* **131**, 4085-4093.

Supp, D. M., Witte, D. P., Potter, S. S. and Brueckner, M. (1997). Mutation of an axonemal dynein affects left-right asymmetry in inversus viscerum mice. *Nature* **389**, 963-966.

Tabin, C. J. and Vogan, K. J. (2003). A two-cilia model for vertebrate left-right axis specification. *Genes Dev.* **17**, 1-6.

Takeyasu, K., Tamkun, M. M., Renaud, K. J. and Fambrough, D. M. (1988). Ouabain-sensitive (Na+ + K+)-ATPase activity expressed in mouse L cells by transfection with DNA encoding the alpha-subunit of an avian sodium pump. *J. Biol. Chem.* **263**, 4347-4354.

Taulman, P. D., Haycraft, C. J., Balkovetz, D. F. and Yoder, B. K. (2001). Polaris, a protein involved in left-right axis patterning, localizes to basal bodies and cilia. *Mol. Biol. Cell* **12**, 589-599.

Thisse, C. and Thisse, B. (1998). High resolution whole-mount in situ hybridization. *The Zebrafish Science Monitor* **5**, 8-9.

Thompson, J. D., Higgins, D. G. and Gibson, T. J. (1994). CLUSTAL W: improving the sensitivity of progressive multiple sequence alignment through sequence weighting, position-specific gap penalties and weight matrix choice. *Nucleic Acids Res.* **22**, 4673-4680.

Tsujikawa, M. and Malicki, J. (2004). Intraflagellar transport genes are essential for differentiation and survival of vertebrate sensory neurons. *Neuron* **42**, 703-716.

Westerfield, M. (1995). *The Zebrafish Book*. Eugene: University of Oregon Press.

White, H. L. (1929). Some measurements of ciliary activity. *Am. J. Physiol.* **88**, 282-285.

Woolf, A. S., Price, K. L., Scambler, P. J. and Winyard, P. J. (2004).

Evolving concepts in human renal dysplasia. *J. Am. Soc. Nephrol.* **15**, 998-1007.

Worthington, W. C., Jr and Cathcart, R. S., 3rd. (1963). Ependymal cilia: distribution and activity in the adult human brain. *Science* **139**, 221-222.

Worthington, W. C., Jr and Cathcart, R. S., 3rd. (1966). Ciliary currents on ependymal surfaces. *Ann. New York Acad. Sci.* **130**, 944-950.

Yan, Y. T., Gritsman, K., Ding, J., Burdine, R. D., Corrales, J. D., Price, S. M., Talbot, W. S., Schier, A. F. and Shen, M. M. (1999). Conserved requirement for EGF-CFC genes in vertebrate left-right axis formation. *Genes Dev.* **13**, 2527-2537.

Yoder, B. K., Hou, X. and Guay-Woodford, L. M. (2002). The polycystic kidney disease proteins, polycystin-1, polycystin-2, polaris, and cystin, are co-localized in renal cilia. *J. Am. Soc. Nephrol.* **13**, 2508-2516.

Yoder, B. K., Richards, W. G., Sweeney, W. E., Wilkinson, J. E., Avener, E. D. and Woychik, R. P. (1995). Insertional mutagenesis and molecular analysis of a new gene associated with polycystic kidney disease. *Proc. Assoc. Am. Physicians* **107**, 314-323.

Zhang, X. M., Ramalho-Santos, M. and McMahon, A. P. (2001). Smoothened mutants reveal redundant roles for Shh and Ihh signaling including regulation of L/R symmetry by the mouse node. *Cell* **106**, 781-792.

Zimmermann, H. D. (1971). Cilia in the fetal kidney of man. *Beitr. Pathol.* **143**, 227-240.